NOTES AND CORRESPONDENCE

Impact of Great Salinity Anomalies on the Low-Frequency Variability of the North Atlantic Climate

RONG ZHANG AND GEOFFREY K. VALLIS

Geophysical Fluid Dynamics Laboratory, and Atmospheric and Oceanic Sciences Program, Princeton University, Princeton, New Jersey

(Manuscript received 25 April 2005, in final form 4 August 2005)

ABSTRACT

In this paper, it is shown that coherent large-scale low-frequency variabilities in the North Atlantic Ocean—that is, the variations of thermohaline circulation, deep western boundary current, northern recirculation gyre, and Gulf Stream path—are associated with high-latitude oceanic Great Salinity Anomaly events. In particular, a dipolar sea surface temperature anomaly (warming off the U.S. east coast and cooling south of Greenland) can be triggered by the Great Salinity Anomaly events several years in advance, thus providing a degree of long-term predictability to the system. Diagnosed phase relationships among an observed proxy for Great Salinity Anomaly events, the Labrador Sea sea surface temperature anomaly, and the North Atlantic Oscillation are also discussed.

1. Introduction

It has long been controversial as to whether the observed low-frequency variabilities in the North Atlantic Ocean, such as sea surface temperature (SST) anomalies (Deser and Blackmon 1993; Kushnir 1994) and Gulf Stream path shifts (Taylor and Stephens 1998; Joyce et al. 2000) are directly forced by the atmospheric North Atlantic Oscillation (NAO; Hurrell 1995), as suggested by Halliwell (1997) and Eden and Jung (2001), or whether the low-frequency NAO variability is modulated by North Atlantic oceanic variability (Rodwell et al. 1999; Mehta et al. 2000; Robertson et al. 2000; Latif 2001). A third option is that such variability is caused by ocean–atmosphere coupled oscillations (Delworth et al. 1993; Joyce et al. 2000). Here we show that the North Atlantic low-frequency variations are closely related to the Great Salinity Anomalies (GSAs). A strong GSA event occurred in the 1970s, when anomalous freshwater/sea ice from the Arctic ocean propagated into the North Atlantic subpolar gyre (Dickson et al. 1988). The GSA events reoccurred during the 1980s and 1990s (Belkin et al. 1998; Belkin 2004). There are also observational indications for the occurrence of GSA events during the early twentieth century (Dickson et al. 1988; Walsh and Chapman 1990; Schmith and Hansen 2003).

During GSA events, low-salinity water propagates into Labrador Sea and reduces the deep water formation there (Lazier 1980). For example, the observed reductions of Labrador Seawater thickness during the 1970s and 1980s (Curry et al. 1998) are related to GSA events. The reduction of Labrador Sea deep water formation will lead to a weakening of the thermohaline circulation (THC) and deep western boundary current (DWBC; Fig. 1). Previous modeling studies showed that the THC can be weakened by the negative polar surface salinity anomalies (Delworth et al. 1993; Häkkinen 1993; Weaver et al. 1993). The modeling result of Thompson and Schmitz (1989) showed that the Gulf Stream at the separation point is influenced by the DWBC. However, this seems inconsistent with observations that there is little change in the separation point at Cape Hatteras on decadal time scales; rather, observations show that major decadal shifts of the Gulf Stream path occurred in the open ocean downstream of Cape Hatteras (Joyce et al. 2000). Zhang and Vallis (2005, manuscript submitted to *J. Phys. Oceanogr.*)

Corresponding author address: Rong Zhang, GFDL/AOS Program, Princeton University, Princeton, NJ 08542.
E-mail: rong.zhang@noaa.gov

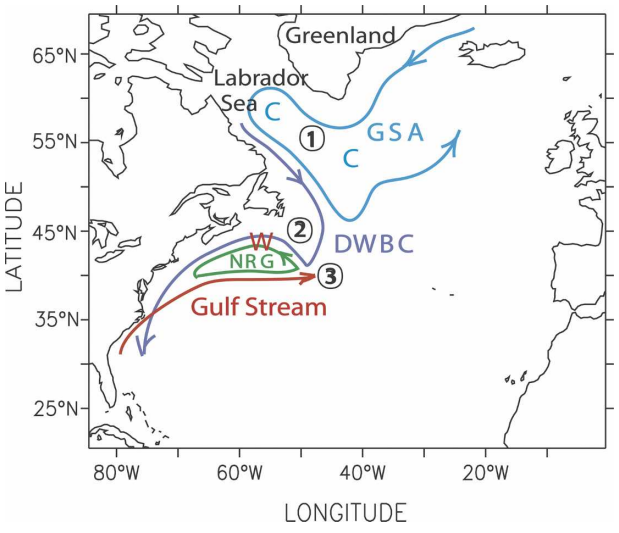

FIG. 1. Schematic diagram of the mechanism: 1) propagation of GSA, 2) weakening of DWBC, and 3) weakening of NRG and a northward shift of mean Gulf Stream path. Here, "W" indicates warming and "C" indicates cooling.

showed that the bottom vortex stretching induced by the downslope DWBC over the steep continental slope south of the Grand Banks influences the formation of the observed cyclonic northern recirculation gyre (NRG) north of the Gulf Stream and keeps the Gulf Stream path downstream of Cape Hatteras separated from the coast. Hence, as the weakened DWBC arrives south of the Grand Banks a few years later, the bottom vortex stretching effect is weakened, resulting in the weakening of the NRG, a northward shift of Gulf Stream path, and warming off the U.S. east coast. Meanwhile the propagation of the low-salinity anomaly in the subpolar gyre induces widespread cooling south of Greenland. Thus a dipolar SST anomaly appears in the North Atlantic. In this study, we simulate the above proposed processes with a numerical model.

Such phenomena may have important climate ramifications. For example, Rodwell et al. (1999) showed that positive phases of the NAO at decadal or longer time scales can be forced by a dipolar SST anomaly (warming off the U.S. east coast and cooling south of Greenland). We show that just such a dipolar SST anomaly could be triggered by GSA events that occur some years in advance and therefore that GSA events could lead to changes in the phase of the NAO at very long time scales. However, there is still much debate as to whether the oceanic forcing of NAO found by Rodwell et al. (1999) is a real effect—many modeling studies with atmosphere general circulation models (AGCMs) show a weak response of NAO to extratropical SST forcing (Kushnir et al. 2002). Mehta et al. (2000) did reproduce the results of Rodwell et al. (1999) with a different AGCM and showed that the correlation between simulated ensemble-mean NAO index (forced by observed SST anomaly) and observed NAO index is much higher for low-pass-filtered data than for unfiltered data. The ensemble averaging considerably reduces variability of the averaged sea level pressure (SLP) anomalies; hence, the simulated ensemble average NAO is considerably weaker than the observed NAO (Mehta et al. 2000). These AGCM simulations do suggest that the SST anomaly can modulate the phase of NAO at low frequency, while the physical processes that control the amplitudes of NAO are not well simulated. Nevertheless, given the doubt as to the possible influence of the ocean on the atmosphere, we explore the influence of GSA events on North Atlantic climate variability with diagnoses of observed datasets of the twentieth century.

2. Modeling the oceanic impacts of GSA events

a. Model setup and experimental design

We model impacts of GSAs on the low-frequency variability in the North Atlantic with a $1° \times 1°$ global ocean general circulation model (OGCM)—the Geophysical Fluid Dynamics Laboratory (GFDL) Modular Ocean Model, version 4 (MOM4; Griffies et al. 2004) coupled to an atmospheric energy balance model (EBM) with a hydrological cycle and a slab sea ice model (Winton 2000). This class of models provides a useful and appropriate way to study the ocean's low-frequency variability, free from the complications of using a full atmospheric GCM, yet allowing large-scale atmospheric feedbacks to THC variations that are not available with ocean-only models (e.g., Weaver et al. 2001). The coupled model is spun up for 51 yr with Comprehensive Ocean–Atmosphere Data Set (COADS; da Silva et al. 1994) climatological monthly mean surface wind stress and wind speed. The THC (maximum meridional overturning streamfunction in the North Atlantic) is stabilized after the spinup, although the spinup time is not long enough for the entire deep ocean to reach equilibrium. This time scale is long enough for the adjustment of DWBC in the western North Atlantic and upper-ocean properties in the North Atlantic, which we focus on here. Gerdes and Köberle (1995) showed that the western boundary region in the North Atlantic deep ocean reaches near steady state within an adjustment period of 10 yr in response to the surface buoyancy forcing in deep-water formation regions. This adjustment time scale of the western boundary region in the North Atlantic deep

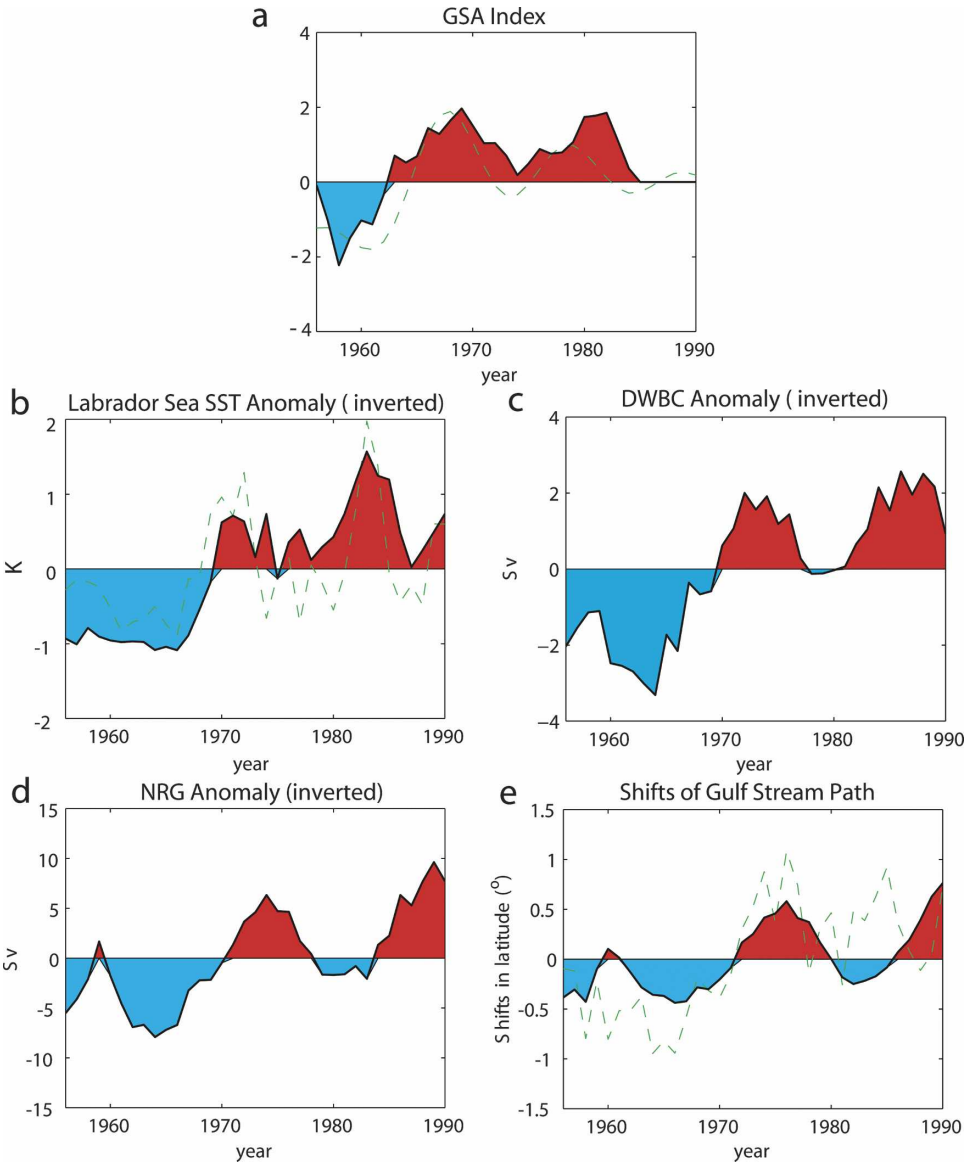

FIG. 2. Modeling results with all anomalous forcings (GW + WIND + GSA). (a) GSA index (color shade) and low-pass-filtered observed Iceland sea ice extent anomaly (green dashed line), normalized by their std devs. (b) Modeled (inverted) central Labrador Sea SST anomaly (K; red means cooling) and observed (inverted) anomaly (K; green dashed line; HadISST). (c) Modeled (inverted) DWBC anomaly at 44°N (Sv; red means less southward transport). (d) Modeled NRG anomaly [Sv; inverted, i.e., the anomaly of the barotropic streamfunction at the center of the NRG (41°N, 57°W); red means weakening, less cyclonic]. (e) Modeled shifts of mean Gulf Stream path in degrees and that diagnosed from *WOD98* (green dash line), i.e., the averaged location of the annual mean 15°C isotherm at 200 m between 75° and 55°W.

ocean depends on the advection time scale of DWBC from deep-water formation source regions, not the background diffusive time scale. The coupled model is integrated continuously for another 45 yr as a control experiment. The model produces a cyclonic NRG and a separated Gulf Stream path downstream of Cape Hatteras from the coast in the mean-state ocean circulation (Zhang and Vallis 2005, manuscript submitted to *J. Phys. Oceanogr.*).

We simulate GSA events by adding a time series of anomalous freshwater flux over the past several decades (Fig. 2a; "GSA index") near the Greenland coast in the model, assuming that it is proportional to observed SLP difference (COADS; da Silva et al. 1994)

between the Labrador Sea off the Greenland west coast (63°N, 56°W) and the Arctic north of the Kara Sea (78°N, 75°E), smoothed with a 5-yr running mean. The two locations were chosen because the observed SLP anomaly there has the maximum positive and negative covariance, respectively, with the Iceland sea ice extent anomaly (Fig. 2a) over the past several decades. The Iceland sea ice extent anomaly is derived from one of the long-term Icelandic sea ice records, the number of areas off the coasts of Iceland on which sea ice is observed in a sea ice year as defined and recorded in Wallevik and Sigurjónsson (1998). It is very similar to another long-term Icelandic sea ice record, the well-known Koch index (Kelly et al. 1987), which is defined as the number of weeks any sea ice is observed near the coasts of Iceland in a sea ice year. The sea ice year is defined in terms of the normal cycle of ice advance and retreat, October–September, and is dated by the year of the January. These long-term Icelandic sea ice records are maintained by the Icelandic Meteorological Office (Wallevik and Sigurjónsson 1998). During the "GSA'70" event, anomalous sea ice exported from the Arctic entered into the North Atlantic through the Denmark Strait off the Icelandic coast (Dickson et al. 1988). Walsh and Chapman (1990) used the Koch index as a proxy for the GSA events. Similarly, the GSA index we used in the simulations correlates with the Iceland sea ice extent anomaly. We do note that the GSAs are not necessarily caused solely by the anomalous freshwater and sea ice from the Arctic via the Fram Strait. Local forcing over the Labrador Sea region is important in causing the "GSA'80" and "GSA'90" events as shown in Belkin et al. (1998) and Belkin (2004). Hence, the Iceland sea ice extent anomaly underestimates the strength of GSA'80 and GSA'90.

Walsh and Chapman (1990) also suggested that GSA events are correlated with the difference of SLP anomaly between the Greenland and the Arctic. The GSA index used in our simulations represents both the remote forcing from the Arctic north of the Kara Sea and the local forcing from the Labrador Sea off the Greenland west coast for GSA events. Its amplitude is based on the estimated anomalous freshwater flux entering the North Atlantic during the GSA'70 (Dickson et al. 1988). We focused on the GSA'70 and GSA'80 events (positive phases around late 1960s and late 1970s in the GSA index and observed Iceland sea ice extent anomaly; Fig. 2a); no anomalous freshwater flux is applied after 1984.

We perform several perturbed experiments (listed in Table 1) with various combinations of the anomalous external forcing, including those due to the increase of atmospheric greenhouse gases and COADS anomalous wind forcing ("GW + WIND"), as well as the above-mentioned anomalous freshwater flux forcing due to GSA events ("GSA"), for a 45-yr period from January 1946 to December 1990. The temporal variation of the difference between each perturbed experiment and the control experiment for the 45-yr period is calculated to represent the response to various anomalous external forcing, similar to the method used in Manabe et al. (1990). We discard the first 10 years of the integrations to avoid the initial shock in changing the wind forcing from the climatological values, and we analyze the period of 1956–90. To compare with observations, we define the "climatology" as the average for the 35-yr period of 1956–90. All anomalous responses shown below are relative to the defined climatology.

TABLE 1. List of perturbed experiments.

Anomalous external forcing	GW	GW + WIND	GSA	GW + WIND + GSA
Anomalous radiative forcing	X	X		X
Anomalous wind forcing		X		X
Anomalous freshwater forcing			X	X

b. Model results

We found that, typically, anomalous radiative forcing due to increased greenhouse gases has little impact on the North Atlantic decadal variations as compared with that of other forcings. For the experiment forced only with the COADS anomalous wind forcing and the anomalous radiative forcing due to increased greenhouse gases (GW + WIND), that is, the anomalous freshwater flux is not included, the modeled anomalous freshwater export from the Arctic through the Fram Strait is very small and is negligible when compared with that found in Häkkinen (1993). This is mainly because the COADS anomalous wind forcing does not contain adequate data over the Arctic region, and thus the experiment cannot simulate well the wind-driven freshwater transport through the Fram Strait. Hence, the above experiment (GW + WIND) cannot obtain the GSA forcing, and we included the anomalous freshwater flux (Fig. 2a) in experiments (GSA and "GW + WIND + GSA") to represent the total anomalous freshwater flux entering into the North Atlantic as a result of GSA events. Note that we do not try to model the root cause of GSA events; rather, we impose the anomalous freshwater flux entering into the North Atlantic as a result of GSA events.

With all anomalous forcings (anomalous radiative forcing due to increased greenhouse gases, COADS

TABLE 2. Modeled decadal anomalies.

Modeled decadal anomalies	GW + WIND	GSA	GW + WIND + GSA
Labrador Sea SST anomaly in 1970 (K)	0.04	−0.45	−0.62
Labrador Sea SST anomaly in 1983 (K)	−0.17	−1.23	−1.57
Max DWBC weakening in the 1970s (Sv)	1.3	1.0	2.0
Max DWBC weakening in the 1980s (Sv)	1.0	1.6	2.6
Max NRG weakening in the 1970s (Sv)	4.0	2.7	6.3
Max NRG weakening in the 1980s (Sv)	2.5	4.7	9.6
Max northward Gulf Stream shift in the 1970s (°)	0.37	0.22	0.58
Max northward Gulf Stream shift in the 1980s (°)	0.29	0.24	0.76

anomalous wind forcing, and the anomalous freshwater flux forcing due to GSA events; GW + WIND + GSA) together, the modeled SST anomaly in the Labrador Sea shows significant cooling in the early 1970s and early 1980s; for example, the anomalous cooling reaches 0.62 K in 1970 and 1.57 K in 1983, respectively, similar to the observed cooling [Fig. 2b; Hadley Centre Sea Ice and Sea Surface Temperature (HadISST) dataset; Rayner et al. 2003]. For the experiment (GSA) forced only with the anomalous freshwater flux due to GSA events (Fig. 2a), the modeled SST anomaly in the Labrador Sea shows cooling of 0.45 K in 1970 and 1.23 K in 1983, respectively (Table 2). For the experiment (GW + WIND) forced only with the COADS anomalous wind forcing and the anomalous radiative forcing due to increased greenhouse gases, the modeled SST anomaly in the Labrador Sea shows 0.04 K warming in 1970 and 0.17 K cooling in 1983, respectively (Table 2). Hence, the modeled Labrador Sea cooling in the early 1970s and early 1980s is mainly due to GSA'70 and GSA'80 events.

With all anomalous forcings (GW + WIND + GSA), the modeled DWBC near the Grand Banks, cyclonic NRG (Figs. 2c,d), and maximum THC are weakened in the mid-1970s and mid- to late 1980s. The modeled mean Gulf Stream path shifts to the north in the mid-1970s and around 1990, which is also shown in diagnoses from the *World Ocean Database 1998* (*WOD98*; Levitus et al. 1998; Fig. 2e). The modeled total weakening of NRG is consistent with interpentadal variations of NRG diagnosed from observations (Greatbatch et al. 1991; Ezer et al. 1995). The contributions from GSA events and the anomalous wind forcing to the total weakening of DWBC, THC, and NRG and northward shifts of mean Gulf Stream path are on the same order. For the experiment (GW + WIND) forced only with the COADS anomalous wind forcing and the anomalous radiative forcing due to increased greenhouse gases, the modeled DWBC is weakened by a maximum of 1.3 Sv (1 Sv $\equiv 10^6$ m^3 s^{-1}) in 1972 and 1.0 Sv in 1984, the modeled NRG is weakened by a maximum of 4.0 Sv in 1974 and 2.5 Sv in 1986, and the modeled mean Gulf Stream path shifts northward by a maximum of 0.37° in 1976 and 0.29° in 1990 (Table 2). These responses are mainly due to the reduced wind speed over the Labrador Sea during negative NAO phases at 1970 and 1980, respectively, which induces a reduction of outgoing surface heat flux, a weak surface warming, and weakened deep-water formation, resulting in the weakening of THC, DWBC, and NRG and northward shifts of Gulf Stream path several years later. The increased greenhouse gases also contribute to the long-term weakening trend of the THC/DWBC in the above experiment (GW + WIND). For example, for the experiment ("GW") forced with only the anomalous radiative forcing due to increased greenhouse gases, the DWBC is linearly reduced by 0.86 Sv from 1956 to 1990. For the experiment (GSA) forced only with the anomalous freshwater flux due to GSA events (Fig. 2a), the modeled DWBC is weakened by a maximum of 1.0 Sv in 1973 and 1.6 Sv in 1985, the modeled NRG is weakened by a maximum of 2.7 Sv in 1974 and 4.7 Sv in 1987, and the modeled mean Gulf Stream path shifts northward by a maximum of 0.22° in 1976 and 0.24° in 1989 (Table 2).

The modeled northward shifts of the mean Gulf Stream path (Fig. 2e) lag the weakening of NRG (Fig. 2d) by 1 yr at the maximum correlation ($r = 0.87$) because of the westward propagation of Rossby waves excited by DWBC variations south of Grand Banks and thus may lag the warming off the U.S. east coast induced by the weakening of the cyclonic NRG. Indeed, both observation (*WOD98*) and modeling results (Fig. 3) show that a large-scale dipole pattern (warming off the U.S. east coast and cooling south of Greenland) leads the northward shift of the mean Gulf Stream path by about 1 yr. This dipole pattern with the warming confined to NRG region is different from typical NAO-forced tripolar pattern (Kushnir et al. 2002) induced directly by the wind and the low-frequency NAO-forced one-sign monopole pattern of SST anomaly (Visbeck et al. 1998), indicating that it is not only forced

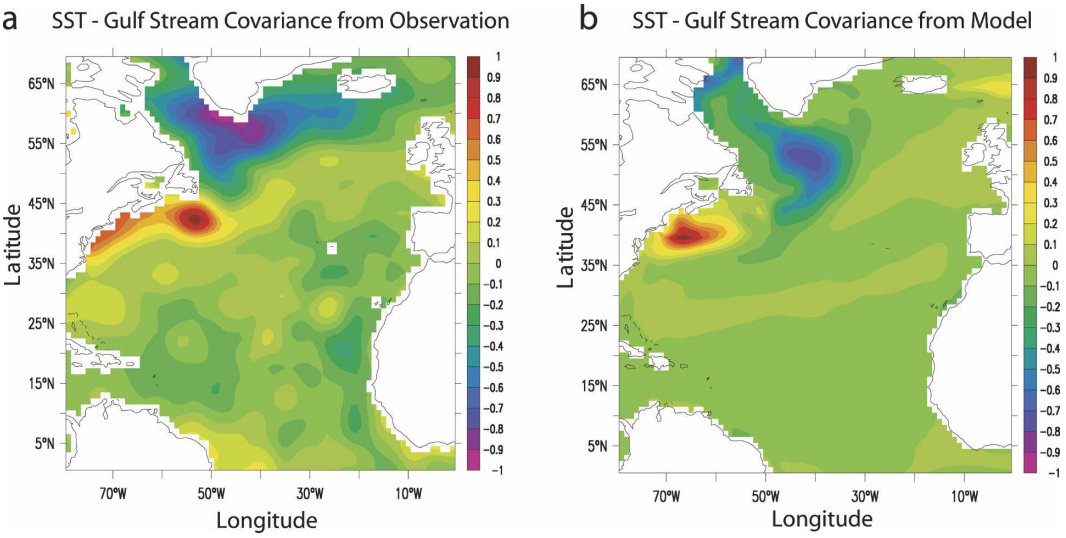

FIG. 3. Normalized covariance between SST anomaly and 1-yr lagged shifts of Gulf Stream path (1956–90). (a) Diagnosed from observations (*WOD98*). (b) Results from the numerical experiment with all anomalous forcings (GW + WIND + GSA). The difference between the integration of covariance over the domain off the U.S. east coast (38°–43°N, 70°–52°W) and over the domain south of Greenland (48°–60°N, 48°–38°W) reaches the maximum when shifts of Gulf Stream path lagged the SST anomaly by about 1 yr in both observation and modeling results.

by the wind. The cooling south of Greenland is mainly due to the propagation of low-salinity anomaly in the subpolar gyre. The warming off the U.S. east coast is not forced by air–sea heat flux, but is due to variations of oceanic advection associated with the weakening of NRG. The atmosphere provides negative feedback to this dipole SST anomaly; that is, more surface heat flux enters into the subpolar North Atlantic, and less surface heat flux is released into the atmosphere off the U.S. east coast, indicating a reduced poleward oceanic heat transport, consistent with the weakening of THC. The differences between the modeled and observed dipole pattern (Fig. 3) are mainly due to the model biases in the mean state ocean circulation. For example, in the modeled mean state, the part of NRG south of Newfoundland is too weak compared to observations; thus the warming there associated with the weakening of the NRG is very small (Fig. 3b), while the observed warming off the U.S. east coast extends farther eastward to south of Newfoundland (Fig. 3a); the modeled cooling south of Greenland does not extend as wide as that observed (Fig. 3), because the modeled mean state subpolar gyre circulation is weaker than observed.

3. Observed relationship between GSA and NAO

Some simulations with atmospheric GCMs (Rodwell et al. 1999; Mehta et al. 2000) suggest that a dipolar SST anomaly pattern (warming off the U.S. east coast and cooling south of Greenland) can modulate the phase of NAO at low frequency, and in particular can efficiently force the low-frequency positive NAO phases. This is by no means the universal response of AGCMs, and other modeling studies with AGCMs show a weak response of NAO to extratropical SST forcing (Kushnir et al. 2002). However, if the dipolar SST anomaly pattern seen in both observations and our numerical results (warming off the U.S. east coast and cooling south of Greenland; Fig. 3) *can* force positive NAO phases at low frequency, then GSA events may lead to positive phases of NAO at low frequency by triggering just such SST anomaly patterns. As noted, this effect is very difficult to reliably model numerically, so we test it with analyses of three independent observed time series of the twentieth century: (i) Iceland sea ice extent anomaly, derived from one of the long-term Icelandic sea ice records, the number of areas off the coasts of Iceland on which sea ice is observed in a sea ice year (Wallevik and Sigurjónsson 1998), by removing the trend for the whole period; (ii) Labrador Sea SST anomaly (HadISST; Rayner et al. 2003); (iii) the NAO index (Hurrell 1995). At decadal or longer time scales, the positive GSA events (more Iceland sea ice extent) occurred in the early twentieth century as well as in the late 1960s and late 1970s, and the negative GSA phase (less Iceland sea ice extent) occurred in the middle twentieth century (Fig. 4a). Both the Labrador Sea surface cooling (warming) and positive (negative) NAO phase (Figs. 4b,c) lagged the positive (negative) GSA events by a few years, respectively. The negative NAO

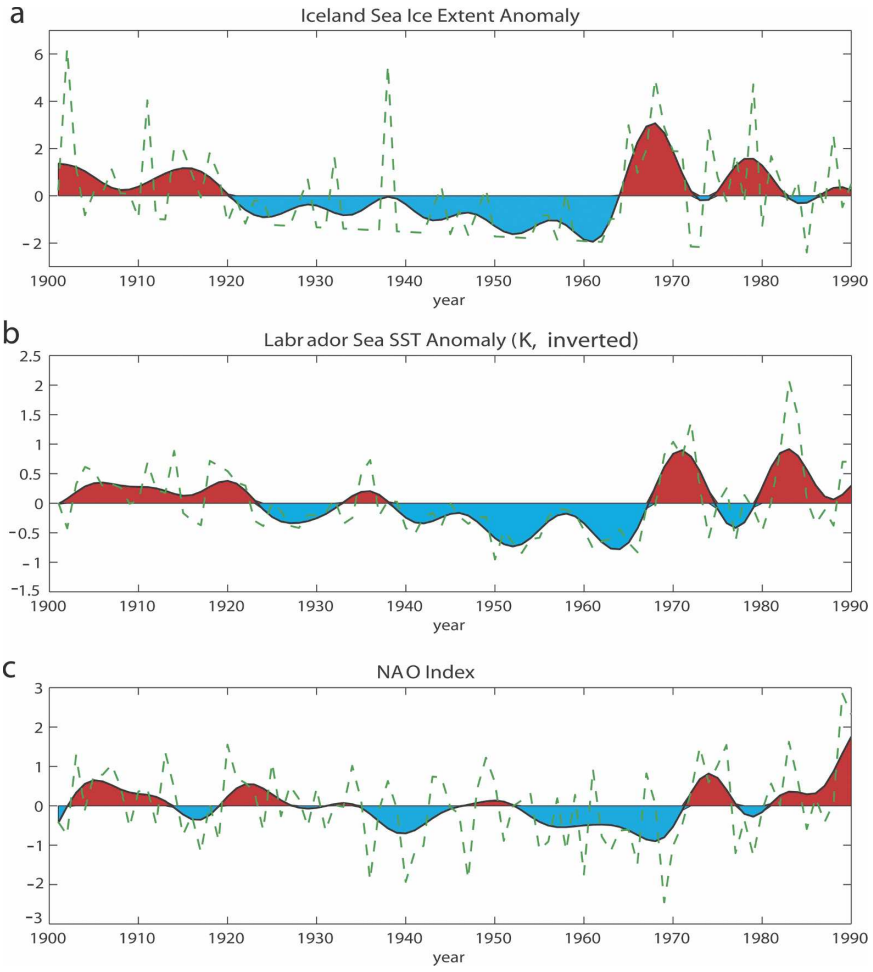

FIG. 4. Observed time series during the twentieth century. (a) Annual Iceland sea ice extent anomaly; the original dataset is maintained by the Icelandic Meteorological Office (Wallevik and Sigurjónsson 1998). (b) Central Labrador Sea (60°N, 55°W) annual mean (inverted) SST anomaly from HadISST dataset (K). (c) Winter (December–March) principal-component-based NAO index (Hurrell 1995, provided by the Climate Analysis Section, NCAR, Boulder, CO). The green dashed line is the unfiltered data, and the color shading is the 8-yr low-pass-filtered data. The linear trends for the whole period (1901–90) of the time series are removed.

trend in the middle twentieth century (before the 1970s; Fig. 4c) cannot be explained by global warming (Hoerling et al. 2001) or stratospheric ozone depletion (Hartmann et al. 2000), and may have been triggered by the negative GSA phase several years prior.

The lag relationship between NAO and GSA events at low frequency is robust throughout the whole period and suggests that there may be some long-term predictability. Indeed at low frequency (Fig. 5a) the positive Iceland sea ice extent anomaly leads the positive NAO phase by 7 yr at the maximum cross correlation (r = 0.66) and leads the Labrador Sea surface cooling by 3 yr ($r = -0.85$); the Labrador Sea surface cooling leads the positive NAO phase by 4 yr ($r = -0.64$). Simulated variables show similar phase relationships (Fig. 5b); that is, the positive GSA index leads modeled Labrador Sea surface cooling by 3 yr ($r = -0.66$), the approximate propagation time scale of the salinity anomaly from east Greenland coast to central Labrador Sea. The positive GSA index also leads the modeled weakening of NRG (Fig. 5b) by 6 yr ($r = 0.78$). The modeled Labrador Sea surface cooling leads the weakening of NRG by 4 yr ($r = -0.7$), that is, the advection time scale of DWBC from the Labrador Sea to south of the Grand Banks. There is almost no lag between modeled NRG anomaly and dipole SST anomaly, and if the dipole SST anomaly can modulate the low-frequency NAO phases (Rodwell et al. 1999), this might provide a mechanism for the observed phase relationships (Fig. 5a).

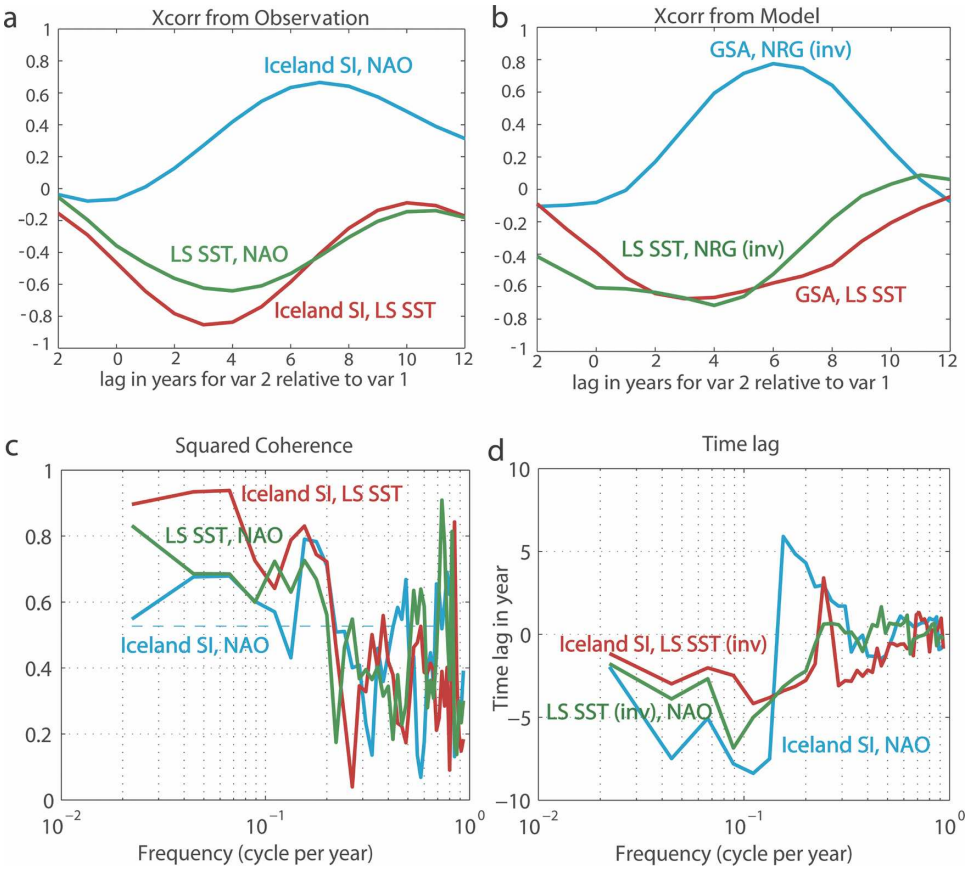

FIG. 5. Cross correlation and cross-spectral analysis of observed variables and comparisons with some modeling results. (a) Cross correlations between low-pass-filtered observed variables shown in Fig. 4. Iceland SI: Iceland sea ice extent anomaly; LS SST: Labrador Sea SST anomaly. (b) Cross correlations between unfiltered modeled variables shown in Fig. 2. NRG (inv): inverted NRG anomaly. (c) Squared coherence between unfiltered observed variables, i.e., the green dashed lines in Fig. 4. The horizontal dashed line is the 95% confidence level. (d) Time lag in years between unfiltered observed variables, i.e., the green dashed lines in Fig. 4. Negative value means that variable 1 leads variable 2. LS SST (inv): inverted Labrador Sea SST anomaly.

Strong coherence (significant at the 95% level) between any two of the above unfiltered observed variables appears at decadal and multidecadal time scales (Fig. 5c). For example, the squared coherence between the unfiltered Iceland sea ice extent anomaly and the NAO index is about 0.59 at decadal time scales (0.1 cycles per year; Fig. 5c) and even higher at longer time scales (the 95% significance level is 0.527). The squared coherence between the unfiltered Labrador Sea SST anomaly and NAO index is slightly stronger, and the squared coherence between the unfiltered Iceland sea ice extent anomaly and the Labrador Sea SST anomaly is even much stronger at the low frequency (Fig. 5c). The cross spectral analysis of unfiltered observed variables also shows that at decadal and multidecadal time scales, the positive (negative) Iceland sea ice extent anomaly leads the Labrador Sea surface cooling (warming) by an average of about 3 yr; the Labrador Sea surface cooling (warming) leads the positive (negative) NAO phase by an average of about 4 yr; the positive (negative) Iceland sea ice extent anomaly leads the positive (negative) NAO phase by an average of about 7 yr (Fig. 5d), consistent with that shown in the Fig. 5a. At interannual time scales, the positive (negative) NAO phase is nearly in phase with the Labrador Sea surface cooling (warming) and the Iceland sea ice extent decrease (increase) (Fig. 5d), that is, the ocean is passively forced by NAO generated by internal atmospheric variabilities (Vallis et al. 2004). At low frequencies the NAO phases are more likely to be influenced by oceanic processes, consistent with a previous study that the correlation between the simulated NAO index

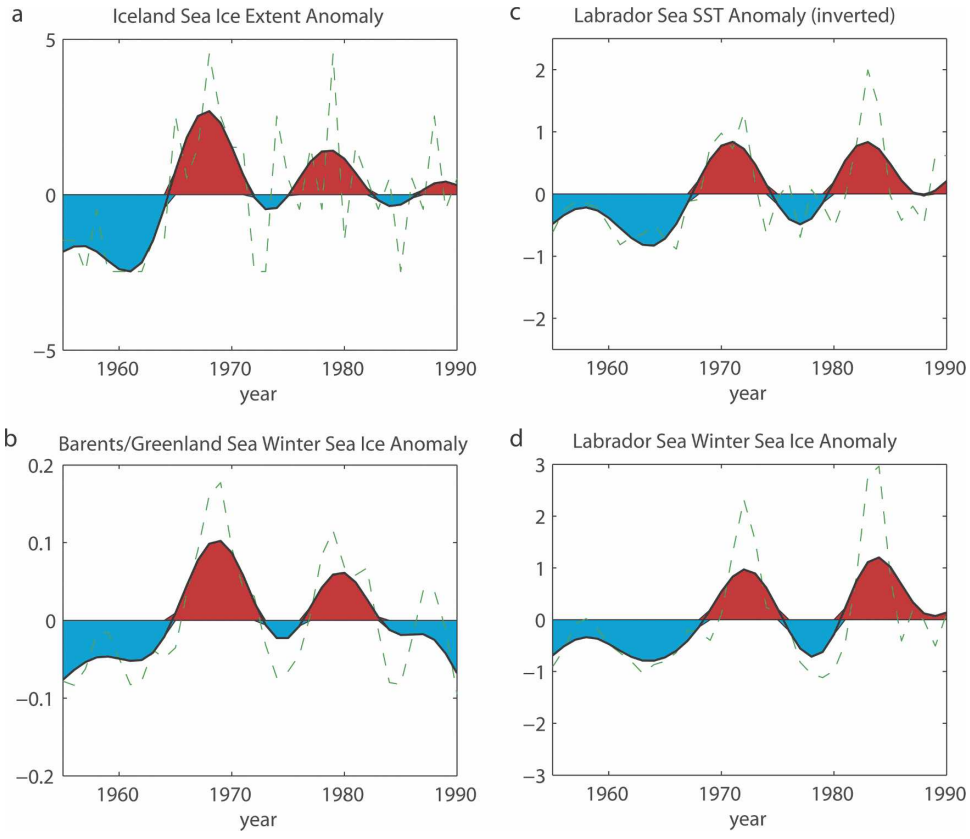

FIG. 6. Comparisons with observed Barents/Greenland Sea and Labrador Sea winter sea ice anomalies. (a) Annual Iceland sea ice extent anomaly; the original dataset is maintained by the Icelandic Meteorological Office (Wallevik and Sigurjónsson 1998). (b) Observed Barents/Greenland Sea (70°–77°N, 10°W–50°E) winter (DJF) sea ice concentration anomaly, plotted in the year in which January occurs. (c) Observed central Labrador Sea (60°N, 55°W) annual mean (inverted) SST anomaly from HadISST dataset (K). (d) Observed Labrador Sea (56°–65°N, 65°–50°W) winter (DJF) sea ice concentration anomaly, plotted in the year in which January occurs. Green dashed line: (a), (c) unfiltered; (b), (d) normalized anomaly smoothed with a three-point binomial filter [for (b) adapted from Fig. 2 and for (d) adapted from Fig. 3 in Deser and Timlin 1996]. Color shading: (a)–(d) 8-yr low-pass filtered.

(forced by observed SST anomaly) and observed NAO index is much higher for low-pass-filtered data than unfiltered data (Mehta et al. 2000).

Similar to the Koch index, the Iceland sea ice extent anomaly we derived from one of the long-term Icelandic sea ice records is a rough estimation of the sea ice severity off the Icelandic coast. To further verify the observed datasets discussed above, we compared them with observations from another independent sea ice data source: the observed Barents/Greenland Sea winter sea ice concentration anomaly (taken from Fig. 2 in Deser and Timlin 1996), and the observed Labrador Sea winter sea ice concentration anomaly (taken from Fig. 3 in Deser and Timlin 1996; also shown in Belkin et al. 1998). We found that at low frequency, the Iceland sea ice extent anomaly (Fig. 6a) is highly correlated ($r = 0.86$) with the observed Barents/Greenland Sea winter sea ice concentration anomaly (Fig. 6b), with a lead of 0–1 yr. The slight time lead is probably because the Iceland sea ice extent anomaly is for annual mean, and the Barents/Greenland Sea winter sea ice anomaly is only for winter [December–February (DJF)]. At low frequency, the increase of Barents/Greenland Sea winter sea ice cover leads the Labrador Sea surface cooling (Fig. 6c) by about 2–3 yr ($r = 0.81$) and leads the positive NAO phase by about 5–6 yr ($r = 0.49$), consistent with the relationship shown in Fig. 5. In the Labrador Sea, surface cooling conditions are associated with high sea ice concentrations (Figs. 6c,d). At low frequency, the observed Labrador Sea SST anomaly we discussed before (Fig. 6c) has very high negative correlation ($r = -0.96$) with the observed Labrador Sea winter sea ice anomaly (Fig. 6d), with a lead of 1 yr. The slight time lead is probably because the SST anomaly is for annual

mean, and the sea ice anomaly is only for winter (DJF). At low frequency, the increase of Iceland sea ice extent leads the increase of the Labrador Sea winter sea ice cover by about 4.5 yr ($r = 0.81$), and the increase of the Labrador Sea winter sea ice cover leads the positive NAO phase by about 2.5 yr ($r = 0.67$). This is also consistent with the relationship shown in Fig. 5.

Deser and Timlin (1996) mentioned the observational evidence that for both of the decadal events in 1) the late 1960s–early 1970s and 2) late 1970s–early 1980s, there was systematic movement of the region of high sea ice concentrations through Denmark Strait around the southern tip of Greenland and into the Labrador Sea, and high sea ice concentrations in Barents/Greenland Sea were followed 3–4 yr later by high sea ice concentrations in the Labrador Sea. These are consistent with the above analysis. A recent observational analysis (Deser et al. 2002) also showed that the freshwater anomalies at 100-m depth in the West Greenland Current preceded the decadal sea ice cover anomaly in the northern Labrador Sea by about 8 months. Note that the positive peak (Figs. 6a,b) in the late 1970s to early 1980s was weaker than that in the late 1960s to early 1970s in both the Iceland sea ice extent anomaly and the Barents/Greenland Sea winter sea ice concentration anomaly; whereas the positive peak (Figs. 6c,d) in the early 1980s is as large as or even stronger than that in the early 1970s in both the Labrador Sea SST anomaly and the Labrador Sea winter sea ice concentration anomaly. This is probably because of the contribution of local forcing to the GSA'80 event (Belkin et al. 1998), and thus the Iceland sea ice extent anomaly and Barents/Greenland Sea winter sea ice concentration anomaly underestimate the strength of the GSA'80 event.

4. Conclusions and discussion

GSA events can evidently play a very important role in causing large-scale coherent low-frequency variabilities in the North Atlantic, such as the weakening of THC, DWBC, and NRG and the northward shifts of mean Gulf Stream path. A large-scale North Atlantic dipolar SST anomaly (warming off the U.S. east coast and cooling south of Greenland), which leads northward shifts of mean Gulf Stream path by about 1 yr, appears in both observations and our modeling results. Such an anomaly is important because some modeling studies (e.g., Rodwell et al. 1999) suggest that it may modulate the phases of NAO at low frequency, although it should also be said that the physical processes that control the amplitudes of NAO are not well understood. If this SST anomaly were driven by unpredictable atmospheric noise, then the system would have no long-term predictability (e.g., Bretherton and Battisti 2000). However, if the SST anomaly were to be triggered by GSA events several years in advance, there would be a degree of long-term predictability to the system. An analysis of long-term observations suggests that, in fact, the latter may be the case: on such long time scales, the positive (negative) Iceland sea ice extent anomaly leads Labrador Sea surface cooling (warming) and the positive (negative) NAO phase by about 3 and 7 yr, respectively, suggesting that the phases of NAO at decadal and multidecadal time scales may be influenced by oceanic processes.

To investigate the oceanic mechanisms involved, we performed various modeling studies, and these show that positive GSA phase typically leads the Labrador Sea surface cooling by about 3 yr and leads the weakening of NRG, which is associated with the dipolar SST anomaly, by about 6 yr. The dipole SST anomaly (warming off the U.S. east coast and cooling south of Greenland) associated with the positive GSA phase, is consistent with a reduction of THC and poleward oceanic heat transport. The atmosphere may have to transport more heat poleward to compensate for the reduced oceanic poleward heat transport, and it is possible that this may lead to more storms and a positive NAO phase. It is not possible to simulate the impact of the dipolar SST anomalies on NAO with the EBM that we used to model the atmosphere, and the precise mechanism whereby oceanic variability affects the atmospheric variability on long time scales is beyond our current scope. The NAO may provide negative feedbacks to GSA events, for example, the decadal oscillations after 1970 may be caused by coupled interactions between NAO and GSAs.

Let us now briefly discuss some of the data used and limitations of our study. The analyzed low-frequency relationship between Barents/Greenland Sea winter sea ice (Labrador Sea winter sea ice anomaly) and the NAO index is based on time series of a relatively short period (1955–90). Observed sea ice data are sparse before the 1950s, and satellite-based sea ice observations are only available after the 1970s. To study the low-frequency North Atlantic variability, especially at the multidecadal time scales, we ideally need very long term observed time series. The records of both the observational-based long-term Iceland sea ice extent anomaly (which is highly correlated with Barents/Greenland Sea winter sea ice anomaly during 1955–90) and the Labrador Sea SST anomaly (which has very strong negative correlation with the Labrador Sea winter sea ice anomaly during 1955–90) go well back before the 1950s; they both indicate that GSA events might

have occurred during the early twentieth century and that they both lead the NAO phases by several years on decadal and multidecadal time scales. Dickson et al. (1988) suggested that the fragmentary ocean data indicate low-salinity events in the North Atlantic during the early twentieth century. The low-frequency variations of the Iceland sea ice extent anomaly (Fig. 4a) are also consistent with a recent reconstruction of the Fram Strait sea ice export (Schmith and Hansen 2003). They found that GSAs observed around 1968–70 and 1980–82 both occurred when the Fram Strait sea ice export was high; prior to these there was a long period with low Fram Strait sea ice export and no GSAs, but early in the nineteenth century several GSAs occurred (Schmith and Hansen 2003). Nevertheless, sea ice extent anomalies along the Icelandic coast may not be always associated with the Arctic sea ice export anomalies. They can be driven by local processes not related to sea ice export anomalies from the Arctic, and they more likely reflect the anomalous sea ice/freshwater entering into the North Atlantic through the Denmark Strait.

Deser and Timlin (1996) showed that the observed high winter sea ice conditions in the Labrador Sea preceded the surface cooling in the North Atlantic subpolar region, consistent with our modeling results that GSA events induce widespread cooling south of Greenland. The multidecadal variations of the Iceland sea ice extent and Labrador Sea SST (Fig. 4) might have contributed to the Atlantic multidecadal oscillation (AMO). The AMO has cool phases in the North Atlantic during 1905–25 and 1970–90, a warm phase in the North Atlantic in the middle twentieth century, and it is thought to be linked to variations in the THC (Delworth and Mann 2000; Enfield et al. 2001). It has been shown that the AMO has significant impacts on the multidecadal climate variability over North America and Europe (Sutton and Hodson 2005), and the multidecadal variability of the Atlantic hurricane activity (Goldenberg et al. 2001). The observed GSA events often refer to positive GSA phases, that is, more sea ice/freshwater and low salinity conditions in the North Atlantic subpolar region. The positive GSA phases that occurred in the early twentieth century as well as those after the 1960s might have contributed to the weakening of THC and the cool AMO phases. The negative GSA phases—that is, periods with less sea ice/freshwater and high-salinity conditions in the North Atlantic subpolar region—are also very important for the North Atlantic low-frequency variability. For example, during the middle twentieth century, the long-term negative GSA phase might have contributed to the long-term Labrador Sea surface warming and the negative NAO trend before the late 1960s with a lead of several years, respectively. The negative GSA phase during the middle twentieth century might have contributed to the strengthening of THC and the warm AMO phase.

In summary, our modeling results suggest that the impact of GSAs (both positive and negative phases), which are often missing in model simulations of North Atlantic low-frequency variability, are at least as important as the impact of the observed anomalous wind forcing for the production of large-scale SST anomalies. The results also suggest that, to simulate the low-frequency temperature variations off the U.S. east coast, it is very important for climate models to properly simulate the mean state NRG and the variations of NRG in response to the variations of DWBC. Of course, the ultimate origin of GSA events is still not very clear. They may originate from coupled interactions of Arctic sea ice, river runoff, and atmospheric and oceanic processes (Mysak et al. 1990), and local processes over the Labrador Sea are also very important (Belkin et al. 1998; Belkin 2004). Evidently, understanding and simulating proper GSA events, and their potential impact on the climate system at large, remains a challenge for climate modeling efforts.

Acknowledgments. We thank Thor Jakobsson at the Icelandic Meteorological Office for providing the observational dataset of the Icelandic Sea Ice records. We also thank Isaac Held for initially providing us with the EBM, Mike Winton for providing us with the sea ice model, and many GFDL colleagues for the development of MOM4 and the Flexible Modeling System (FMS) used in this study. We thank Igor Belkin and an anonymous reviewer for very helpful comments on this paper. The numerical experiments were carried with the supercomputer facilities at NOAA/GFDL, and the work was partially funded by the NSF Ocean Science Division.

REFERENCES

Belkin, I. M., 2004: Propagation of the "Great Salinity Anomaly" of the 1990s around the northern North Atlantic. *Geophys. Res. Lett.,* **31,** L08306, doi:10.1029/2003GL019334.

——, S. Levitus, J. Antonov, and S. Malmberg, 1998: 'Great salinity anomalies' in the North Atlantic. *Progress in Oceanography,* Vol. 41, Pergamon, 1–68.

Bretherton, C. S., and D. S. Battisti, 2000: An interpretation of the results from atmospheric general circulation models forced by the time history of the observed sea surface temperature distribution. *Geophys. Res. Lett.,* **27,** 767–770.

Curry, R. G., M. S. McCartney, and T. M. Joyce, 1998: Oceanic transport of subpolar climate signals to mid-depth subtropical waters. *Nature,* **391,** 575–577.

da Silva, A., A. C. Young, and S. Levitus, 1994: *Algorithms and Procedures.* Vol. 1, *Atlas of Surface Marine Data 1994,* NOAA Atlas NESDIS 6, 83 pp.

Delworth, T. L., and M. E. Mann, 2000: Observed and simulated multidecadal variability in the Northern Hemisphere. *Climate Dyn.,* **16,** 661–676.

——, S. Manabe, and R. J. Stouffer, 1993: Interdecadal variations of the thermohaline circulation in a coupled ocean–atmosphere model. *J. Climate,* **6,** 1993–2011.

Deser, C., and M. L. Blackmon, 1993: Surface climate variations over the North Atlantic ocean during winter: 1900–1989. *J. Climate,* **6,** 1743–1753.

——, and M. S. Timlin, 1996: Decadal variations in sea ice and sea surface temperature in the subpolar North Atlantic. *The Atlantic Climate Change Program, Proc. from the Principal Investigators Meeting,* Woods Hole, MA, WHOI, 36–40.

——, M. Holland, G. Reverdin, and M. Timlin, 2002: Decadal variations in Labrador Sea ice cover and North Atlantic sea surface temperatures. *J. Geophys. Res.,* **107,** 3035, doi:10.1029/2000JC000683.

Dickson, R. R., J. Meincke, S.-A. Malmberg, and A. J. Lee, 1988: The 'Great Salinity Anomaly' in the northern North Atlantic 1968–1982. *Progress in Oceanography,* Vol. 20, Pergamon, 103–151.

Eden, C., and T. Jung, 2001: North Atlantic interdecadal variability: Oceanic response to the North Atlantic Oscillation (1865–1997). *J. Climate,* **14,** 676–691.

Enfield, D. B., A. M. Mestas-Nuñez, and P. J. Trimble, 2001: The Atlantic multidecadal oscillation and its relation to rainfall and river flows in the continental U.S. *Geophys. Res. Lett.,* **28,** 2077–2080.

Ezer, T., G. L. Mellor, and R. J. Greatbatch, 1995: On the interpentadal variability of the North Atlantic Ocean: Model simulated changes in transport, meridional heat flux and coastal sea level between 1955–1959 and 1970–1974. *J. Geophys. Res.,* **100,** 10 559–10 566.

Gerdes, R., and C. Köberle, 1995: On the influence of DSOW in a numerical model of the North Atlantic general circulation. *J. Phys. Oceanogr.,* **25,** 2624–2641.

Goldenberg, S. B., C. W. Landsea, A. M. Mestas-Nuñez, and W. M. Gray, 2001: The recent increase in Atlantic hurricane activity: Causes and implications. *Science,* **293,** 474–479.

Greatbatch, R. J., A. F. Fanning, A. D. Goulding, and S. Levitus, 1991: A diagnosis of interpendatal circulation changes in the North Atlantic. *J. Geophys. Res.,* **96,** 22 009–22 023.

Griffies, S. M., M. J. Harrison, R. C. Pacanowski, and A. Rosati, 2004: A technical guide to MOM4. GFDL Ocean Group Tech. Rep. 5, NOAA/GFDL, 339 pp.

Häkkinen, S., 1993: An Arctic source for the Great Salinity Anomaly: A simulation of the Arctic ice-ocean system for 1955–1975. *J. Geophys. Res.,* **98,** 16 397–16 410.

Halliwell, G. R., Jr., 1997: Decadal and multidecadal North Atlantic SST anomalies driven by standing and propagating basin-scale atmospheric anomalies. *J. Climate,* **10,** 2405–2411.

Hartmann, D. L., J. M. Wallace, V. Limpasuvan, D. W. J. Thompson, and J. R. Holton, 2000: Can ozone depletion and greenhouse warming interact to produce rapid climate change? *Proc. Natl. Acad. Sci. USA,* **97,** 1412–1417.

Hoerling, M. P., J. W. Hurrell, and T. Xu, 2001: Tropical origins for recent North Atlantic climate change. *Science,* **292,** 90–92.

Hurrell, J. W., 1995: Decadal trends in the North Atlantic Oscillation: Regional temperatures and precipitation. *Science,* **269,** 676–679.

Joyce, T. M., C. Deser, and M. A. Spall, 2000: The relation between decadal variability of subtropical mode water and the North Atlantic Oscillation. *J. Climate,* **13,** 2550–2569.

Kelly, P. M., C. M. Goodess, and B. S. G. Cherry, 1987: The interpretation of the Icelandic sea ice record. *J. Geophys. Res.,* **92,** 10 835–10 843.

Kushnir, Y., 1994: Interdecadal variations in North Atlantic sea surface temperature and associated atmospheric conditions. *J. Climate,* **7,** 141–157.

——, W. A. Robinson, I. Bladé, N. M. J. Hall, S. Peng, and R. T. Sutton, 2002: Atmospheric GCM response to extratropical SST anomalies: Synthesis and evaluation. *J. Climate,* **15,** 2233–2256.

Latif, M., 2001: Tropical Pacific/Atlantic ocean interactions at multi-decadal time scales. *Geophys. Res. Lett.,* **28,** 539–542.

Lazier, J. R. N., 1980: Oceanographic conditions at Ocean Weather Ship Bravo, 1964–74. *Atmos.–Ocean,* **18,** 227–238.

Levitus, S., and Coauthors, 1998. *Introduction.* Vol. 1, *World Ocean Database 1998 (WOD98),* 346 pp.

Manabe, S., K. Bryan, and M. J. Spelman, 1990: Transient response of a global ocean–atmosphere model to a doubling of atmospheric carbon dioxide. *J. Phys. Oceanogr.,* **20,** 722–749.

Mehta, V. M., M. J. Suarez, J. V. Manganello, and T. L. Delworth, 2000: Oceanic influence on the North Atlantic Oscillation and associated Northern Hemisphere climate variations: 1959–1993. *Geophys. Res. Lett.,* **27,** 121–124.

Mysak, L. A., D. K. Manak, and D. F. Marsden, 1990: Sea-ice anomalies observed in the Greenland and Labrador Seas during 1901–1984 and their relations to an interdecadal Arctic climate cycle. *Climate Dyn.,* **5,** 111–133.

Rayner, N. A., D. E. Parker, E. B. Horton, C. K. Folland, L. V. Alexander, D. P. Rowell, E. C. Kent, and A. Kaplan, 2003: Global analyses of sea surface temperature, sea ice, and night marine air temperature since the late nineteenth century. *J. Geophys. Res.,* **108,** 4407, doi:10.1029/2002JD002670.

Robertson, A. W., C. R. Mechoso, and Y.-J. Kim, 2000: The influence of sea surface temperature anomalies on the North Atlantic Oscillation. *J. Climate,* **13,** 122–138.

Rodwell, M. J., D. P. Rowell, and C. K. Folland, 1999: Oceanic forcing of the wintertime North Atlantic Oscillation and European climate. *Nature,* **398,** 320–323.

Schmith, T., and C. Hansen, 2003: Fram Strait ice export during the nineteenth and twentieth centuries reconstructed from a multiyear sea ice index from southwestern Greenland. *J. Climate,* **16,** 2782–2791.

Sutton, R. T., and D. L. R. Hodson, 2005: Atlantic ocean forcing of North American and European summer climate. *Science,* **309,** 115–118.

Taylor, A. R., and J. A. Stephens, 1998: The North Atlantic oscillation and the latitude of the Gulf Stream. *Tellus,* **50,** 134–142.

Thompson, J. D., and W. J. Schmitz, 1989: A limited-area model of the Gulf Stream: Design, initial experiments, and model–data intercomparison. *J. Phys. Oceanogr.,* **19,** 791–814.

Vallis, G. K., E. Gerber, P. Kushner, and B. Cash, 2004: A mechanism and simple model of the North Atlantic Oscillation and annular modes. *J. Atmos. Sci.,* **61,** 264–280.

Visbeck, M., H. Cullen, G. Krahmann, and N. Naik, 1998: An

ocean model's response to North Atlantic Oscillation-like wind forcing. *Geophys. Res. Lett.,* **25,** 4521–4524.

Wallevik, J. E., and H. Sigurjónsson, 1998. The Koch Index: Formulation, corrections and extension. Icelandic Meteorological Office Rep. VÍ-G98035-ÚR28, 14 pp.

Walsh, J. E., and W. L. Chapman, 1990: Arctic contribution to upper-ocean variability in the North Atlantic. *J. Climate,* **3,** 1462–1473.

Weaver, A. J., J. Marotzke, P. F. Cummins, and E. S. Sarachik, 1993: Stability and variability of the thermohaline circulation. *J. Phys. Oceanogr.,* **23,** 39–60.

——, and Coauthors, 2001: The UVic Earth System Climate Model: Model description, climatology and application to past, present and future climates. *Atmos.–Ocean,* **39,** 361–428.

Winton, M., 2000: A reformulated three-layer sea ice model. *J. Atmos. Oceanic Technol.,* **17,** 525–531.